Express Polymer Letters Vol.18, No.12 (2024) 1265–1276
Available online at www.expresspolymlett.com
https://doi.org/10.3144/expresspolymlett.2024.94

Research article

Fabricating multifunctional PLA textiles with advanced respiratory detection and environmental safety

Yunhui Wu[1], *Chengkai Luo*[1], *Huanyu Liu*[1], *Wen Li*[1], *Jun-Wei Zha*[2,3*]

[1]Dongguan University of Technology, 523808 Dongguan, P. R. China
[2]Beijing Advanced Innovation Center for Materials Genome Engineering, School of Chemistry and Biological Engineering, University of Science & Technology Beijing, 100083 Beijing, P. R. China
[3]Shunde Innovation School, University of Science and Technology Beijing, 528300 Foshan, P. R. China

Received 6 August 2024; accepted in revised form 26 September 2024

Abstract. Currently, polylactic acid (PLA) is an attractive alternative to polypropylene (PP) because of its biodegradability. This study introduces a novel modification strategy for PLA by creating a multifunctional ionization layer with ionic salts. This approach achieves humidity sensing, reliable antibacterial properties, and excellent degradability simultaneously. The modified PLA textile sensor exhibits high sensitivity to respiratory humidity (0.92 at 90% *RH*), with ultrafast response (0.12 s) and recovery times (0.16 s). Additionally, the textile demonstrates excellent antibacterial performance against both *E. coli* (99.9%) and *S. aureus* (99.9%) after 1 h of contact. It also shows notable biodegradability with a weight loss rate of 60.38% after 30 days. Also, the ionic salt mechanism is explained through dynamic ionization interactions attributed to the modified ionic salts, which feature both long-chain alkanes and active ions. This work presents a new method to enhance the respiratory detection and antibacterial performance of biodegradable masks.

Keywords: *flexible sensor, textile, polymer composites, PLA, ionic salt*

1. Introduction

Since the outbreak of COVID-19 was declared a public health emergency of international concern (PHEIC) on 30 January 2020, the number of confirmed cases has increased exponentially worldwide [1, 2]. The rapid spread and infectious nature of the disease have put people in an unprecedentedly vulnerable situation, leading to a significant rise in the demand for surgical masks [3–8]. Masks are widely used personal protective equipment designed to reduce exposure to bacteria, with more than 4 billion consumed daily [9–12]. However, the increased demand and disposal of surgical masks have led to significant economic costs and environmental impacts [13–15]. Currently, the most common type of surgical masks, made from melt-blown polypropylene (PP), has raised concerns about their self-sterilization and safety for prolonged wear [16–18]. Additionally, the disposal and decontamination of masks contribute to the daily burden of 250 000 t of plastic pollution [19]. Given the high economic and environmental costs, it is crucial to develop degradable masks with self-sterilizing properties that are also accessible to the general population on a large scale [3, 10, 20]. To address the shortage, several strategies are being rapidly developed and implemented [21, 22], such as dry heat, chemical treatments, and steam sterilization. However, these methods either reduce the filtration efficiency of the masks or increase the risk of damaging the PP textile. Recent studies have also focused on developing reusable masks by coating their surfaces with metal or metal oxide nanoparticles, such as carbon nanomaterials and graphene [19, 22–25]. However, these approaches

*Corresponding author, e-mail: zhajw@ustb.edu.cn

face the drawback of potential nanoparticle detachment and inhalation due to the incompatibility between the particles and polymers [16, 26, 27].

Respiration is essential for maintaining human life, and exhaled breath can offer valuable health insights as it contains various substances, including water vapor [24, 28–30]. Specifically, fluctuations in humidity during respiration can be linked to numerous illnesses, such as heart disease, pneumonia, bronchitis, and sleep apnea syndrome [31–34]. Additionally, human exhaled air consistently maintains a high relative humidity (*RH)* level (>90%), which remains unaffected by movement, environment, or seasons [35]. Flexible, wearable humidity sensor technologies in [24] surgical masks offer a promising solution for portable health monitoring. Although materials like carbon, metallic oxides, nanophase silicon, supramolecular materials, inorganics, and graphene have been widely used to enhance the humidity response of masks [7, 36, 37], their performance remains suboptimal at high relative humidity, and there is a risk of particles detaching and being inhaled during mechanical shaking. To date, although the quaternary ammonium compounds are widely used antimicrobial materials [24], their application to the mask encountered notable limitations primarily due to the performance decline stemming from a non-bonded, tenuous attachment on the filter surface, and the complexity, inefficiency, and lack of scalability associated with surface modification [38].

In this study, compound ionic salts composed of didodecyldimethylammonium chloride (DDAC) and sodium methanesulfinate (SMS), featuring ammonium and sodium sulfonate groups, respectively, were used to create an ionization layer on polylactic acid (PLA). This novel organic salt modification strategy imparts a positive charge to the PLA textile, endowing it with respiratory detection and excellent self-sterilization capabilities, as well as good biodegradability. Additionally, the mechanism influenced by both the ammonium and sodium sulfonate groups has been thoroughly explained. This approach provides a new solution to enhance the antibacterial and respiratory detection performance of biodegradable masks.

2. Experimental section

2.1. Materials

Didodecyldimethylammonium chloride (DDAC), sodium alpha-olefin sulfonate (SAOS) and sodium methanesulfinate (SMS) were obtained from Shanghai Aladdin Biochemical Technology Co., China. Ethyl alcohol was purchased from Shanghai Co., China. PLA melting non-woven fabrics were acquired from Smartwin Import and Export Trading Co., China. PLA melting non-woven fabrics have an areal density of 32 g/m^2 and a thickness of 0.20±0.01 mm. The average diameter is about 3.9 μm, and the average pore diameter is 22.6 μm.

2.2. Characterization and method

The fabric surface morphology was evaluated by scanning electron microscope (ZEISS, Sigma-300, Germany) equipped with an energy dispersive X-ray analyzer (Bruker, Quantax XFlash SDD 6, Germany). Also, the surface element of samples was analyzed using XPS analysis (Thermo Scientific, K-Alpha, USA). Fourier transform infrared (FTIR) spectra were obtained by a spectrometer (Brooke, Tensor 27, Germany). DSC measurements were obtained by Mettler Instruments (a Netzsch, DSC 214, Germany). The humidity sensing was tested on equipment (KEITHLEY, 6500, USA) in a constant temperature and humidity test chamber. The relative resistance change ($\Delta R/R_0$) can be calculated from Equation (1):

$$\frac{\Delta R}{R_0} = \frac{R - R_0}{R_0} \tag{1}$$

2.3. Humidity sensors fabrication

Both the DDAC and SMS were separately dissolved in 25 ml ethyl alcohol and magnetic stirred for 1 h. Then, PLA non-woven fabric (3×3 cm) was immersed in the solution. The coated fabric was rinsed with ethyl alcohol to remove unbonded DDAC or SMS. After that, the fabric was removed and dried at 40 °C for 8 h. The composition of PLA/DDAC/SMS is shown in Table 1.

2.4. Antimicrobial evaluation

The antibacterial activity of the fabric was quantified according to the procedures of GBT-31402. Before inoculation of the bacteria, the pieces of fabric were disinfected by ultraviolet C irradiation for 1 min. In this test, both Golden-yellow grapes and *E. coli* were used to challenge the control and the coated samples. The pre-cultured bacterial microorganisms were diluted into $6 \cdot 10^4$ colony-forming units (CFU/ml). The 225 ul of microorganism suspension was placed onto the center of the textile (5×5 cm), and then the textile

Table 1. The PLA/DDAC/SMS textiles were obtained in different concentrations of both DDAC and SMS.

Sample code	Ethyl alcohol [ml]	Mass ration of DDAC to ethyl alcohol [mg/ml]	Mass ration of SMS to ethyl alcohol [mg/ml]
PLA/DDAC-1	20	25	0
PLA/DDAC-2	20	50	0
PLA/DDAC-3	20	75	0
PLA/DDAC-4	20	100	0
PLA/DDAC-5	20	125	0
PLA/DDAC/SMS-1	20	25	20
PLA/DDAC/SMS-2	20	25	30
PLA/DDAC/SMS-3	20	25	40
PLA/DDAC/SMS-4	20	25	50
PLA/DDAC/SMS-5	20	25	60

was 'sandwiched' using another identical sample to ensure full contact. After different periods of contact time, the samples were immediately transferred into 10 ml of soya casein digest lecithin polysorbate broth (0.7 wt%) to quench the residual antimicrobial agent. The quenched solution was diluted and plated onto trypticase agar plates. The plates were incubated at 35 °C 48 h, and the number of viable bacterial colonies were used for final analysis.

2.5. Soil burial test and hydrolytic degradation

The natural active soil was applied to assess the soil burial degradability. The natural soil was characterized by a known capacity to retain water and with a specified water content of 45±10%. The pH value of the soil was 6.5–7. PLA fabric was cut into 3×3 cm. Then, samples were weighed and buried in natural soil under aseptic conditions. The samples were weighed both at the beginning of the test and at the end of the test period. The experimental section needs regular watering to maintain the humidity. Soil degradation of all samples was evaluated on days 0, 30, 60 and 90 days. At the end of each testing period, the polymeric materials were prevailed from the soil, washed with distilled water in order to remove adherent soil and dried on filter paper.

For hydrolytic degradation tests, PLA fabric was cut into 3×3 cm. Then, samples were weighed and placed in labeled vials containing 20 ml of phosphate buffer solution (PBS) with a pH of 1 and 12. All samples were evaluated on days 0, 1, 30, and 60 days, and the weight variation (weight ratio: W_m) was determined using Equation (2):

$$W_m = \frac{M_0 - M_1}{M_0} \cdot 100\% \quad (2)$$

where M_0 is the initial mass of samples, and M_1 is the final mass after degradation and drying.

3. Results and discussion

3.1. Construction of multifunctional ionization layer of PLA/DDAC/SMS

The fabrication strategy for the multifunctional ionization layer of PLA/DDAC/SMS is illustrated in Figure 1. Melt-blown PLA serves as the matrix for the surgical mask (Figure 1a), while SMS, which contains a hydrophilic group, and DDAC, which contains an ammonium group, together form the multifunctional ionization layer (Figure 1b). This innovative design results in an all-organic, multifunctional intelligent surgical mask with capabilities for respiratory humidity detection, excellent self-sterilization, and biodegradability, as shown in Figure 1c. The morphology of the textile before and after treatment is depicted in Figure 1d. The untreated fabric has a net structure and a smooth surface with a typical fibril structure. After treatment, the textile becomes rougher, and the net structure is more exposed. Clearly, both DDAC and SMS are integrated into the PLA textile, forming an all-organic layer that enhances compatibility and stability.

To assess the structural reliability of the multifunctional ionization layer, the intrinsic interactions between PLA, DDAC, and SMS are examined in Figure 2. Figure 2a shows that the loading of DDAC and SMS on the PLA textile increases with the concentration of the suspension, demonstrating a positive functional relationship. Additionally, Figure 2b

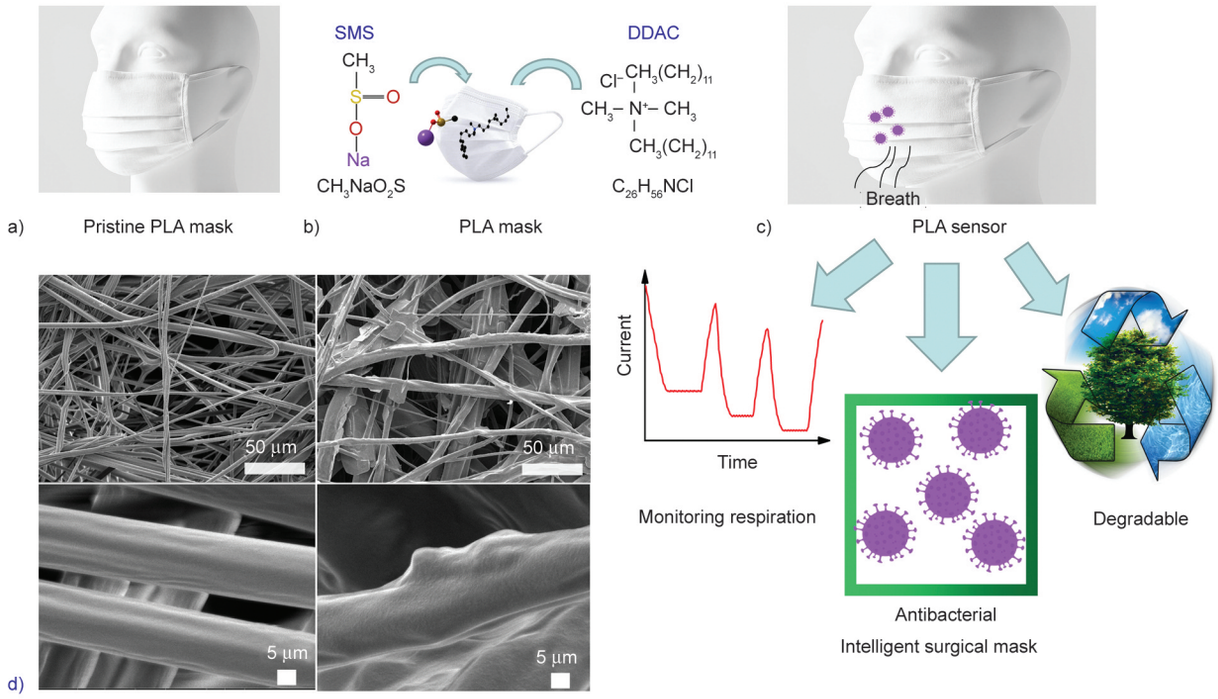

Figure 1. Construction of the PLA/DDAC/SMS intelligent surgical mask sensor. a) Structure diagram of the pristine PLA mask. b) PLA/DDAC/SMS intelligent surgical masks, showing the assembly of DDAC and SMS on the surface of PLA. c) Multifunctional PLA sensor with capabilities for monitoring respiration, antibacterial activity, and degradation. d) Microstructure of the PLA sensor mask, including the PLA textile modified with DDAC and SMS.

presents the correlation between chlorine content and the concentration of DDAC suspension, highlighting its significant impact on antibacterial properties. Figure 2c explores the effect of suspension concentration on hydrophilicity. The untreated PLA fabric has a hydrophobic surface with a water contact angle of approximately 142.9°. However, after coating with DDAC and SMS, the contact angle rapidly decreases to 30°, indicating a complete transformation from hydrophobic to hydrophilic. The hydrophilicity of the PLA/DDAC/SMS mask shows minimal variation, attributed to the sodium ion structure of SMS and its interaction with water. Figures 2d–2f evaluate the breathability and examine the morphological changes of the textile at different DDAC and SMS suspension concentrations. The SEM photograph reveals that the PLA/DDAC/SMS textile maintains better porosity at a low concentration of 20 mg/ml, whereas at concentrations of 30 and 50 mg/ml, the textile becomes partially or completely blocked, respectively. EDS images in Figures 2g–2i show that Cl, S, and Na are evenly distributed on the surface of the PLA textile at the 20 mg/ml concentration. Consequently, the PLA textile treated with a concentration of DDAC (at 25 mg/ml) and SMS (at 20 mg/ml) suspension with average pore diameter PLA/DDAC/SMS is 15.72 μm, which exhibits high hydrophilicity, excellent breathability, and moderate chlorine content, holds significant potential for use in intelligent surgical masks.

To further confirm the effectiveness of the DDAC and SMS coating, the FT-IR results are shown in Figure 2j. In the spectrum of pure PLA, the characteristic absorption peak is located at a wavenumber of 1755 cm^{-1}, corresponding to the C=O stretching vibration. Two absorption bands are observed in the wavenumber range of 1300–1000 cm^{-1}, representing the asymmetric stretching vibration of C–O–C from ester groups. FT-IR results indicate that the coating does not affect the PLA structure. For the PLA/DDAC/SMS spectrum, the peak at 781 cm^{-1} is attributed to the S=O bond from SMS. Two distinct peaks at 2852 and 2920 cm^{-1} are associated with the $–CH_2$ groups in the long alkyl chain from hyamine. Overall, the PLA/DDAC/SMS spectra primarily feature the characteristic peaks of each individual component, suggesting that no chemical reaction occurs between DDAC and SMS; they are physically blended. Additionally, the XPS spectra show that DDAC and SMS are present on the textile (Figure 2k and Figure 2l). Significant peaks at ~200 and ~167 eV are attributed to chloride and sulfide, respectively.

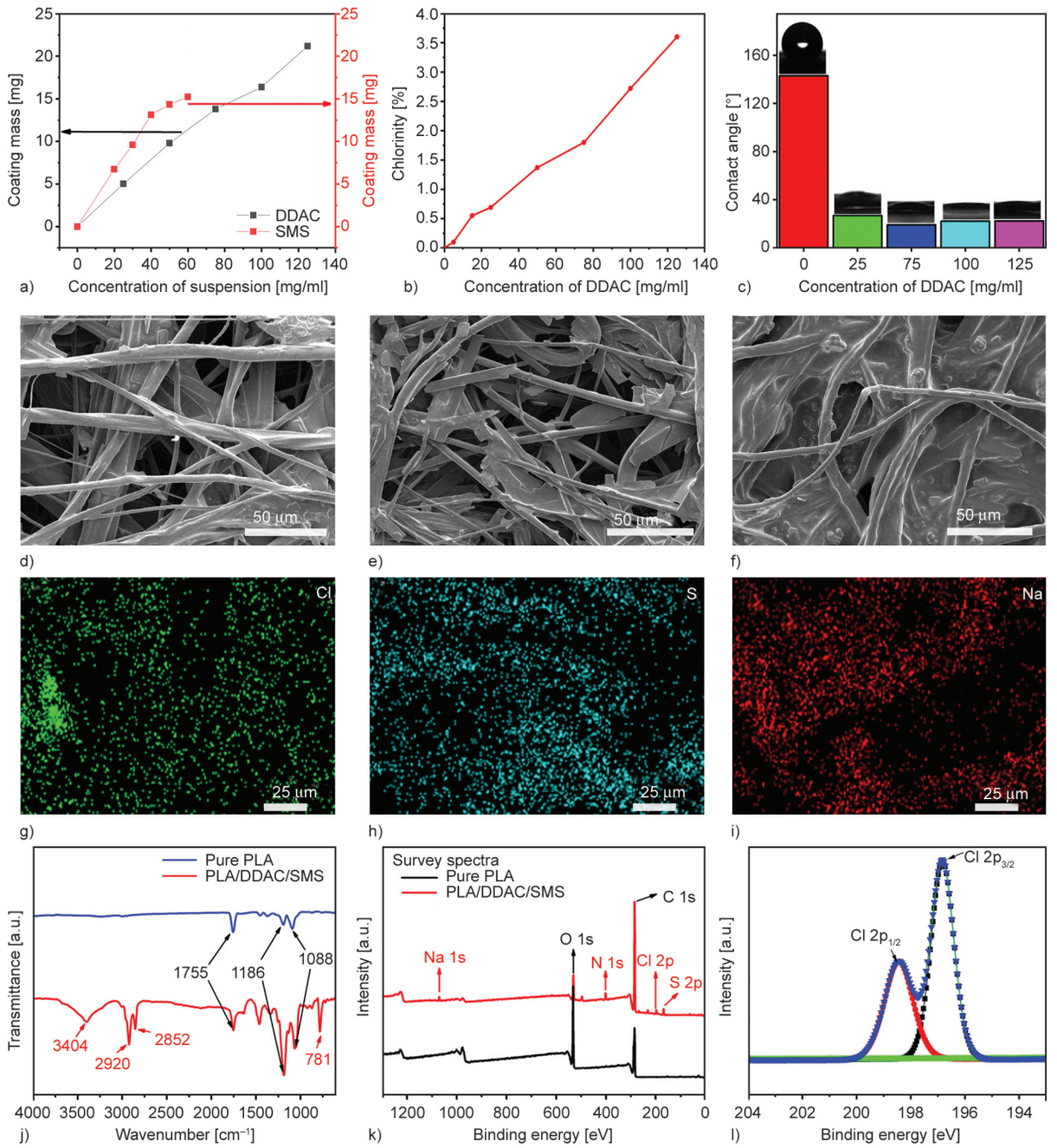

Figure 2. Structure of the PLA/DDAC/SMS intelligent surgical mask sensor. a) Relationship between DDAC and SMS suspension concentration and coating mass (PLA, 10×10 mm, 0.5 g). b) Variation in chlorine content with DDAC suspension concentration. c) Hydrophilic properties as affected by the concentrations of DDAC and SMS suspensions. d)–f) Morphological changes in PLA/DDAC/SMS textile with SMS suspension concentrations of 20, 30, and 50 mg/ml, respectively, with a constant DDAC suspension concentration of 25 mg/ml. g)–i) Representative EDS mapping images showing the distribution of Cl, S, and Na in the coated PLA textile. j) Fourier transform infrared spectroscopy used to track DDAC and SMS on the surface of the PLA mask sensor. k) XPS spectrum investigating the chemical binding energies of chlorine and sodium. l) Cl 2p XPS spectrum of the PLA/DDAC/SMS intelligent surgical mask sensor.

3.2. Sensing mechanism of salt-modified PLA textile

To evaluate the moisture-sensing performance of the multifunctional ionization layer, the effect of DDAC concentration on respiratory detection is examined in Figure 3a. Interestingly, the ability to sustain moisture absorption decreases as DDAC concentration increases. Specifically, the time-dependent $\Delta R/R_0$ variation decreased from 25 to 15 s, 12, 8, and 5 s, respectively. This is mainly due to the occurrence of

the obturator phenomenon in the PLA/DDAC textile at higher concentrations. Subsequently, the highly effective PLA/DDAC-1 is further treated with SMS, as shown in Figure 3b. The time to reach saturation humidity decreases with increasing SMS concentration. To further assess the sensing capability, both $\Delta R/R_0$ and resistance signals are plotted in Figure 3c. It is noted that the sensor exhibits a high humidity sensitivity of 0.92 at *RH* 90%. Resistance variation shows a sensitive dependence on humidity changes, increasing from 50 to 450 kΩ as humidity rises from 30 to 90%.

The sensor demonstrates an ultrafast response time and recovery time of approximately 0.12 and 0.16 s, respectively, as shown in Figure 3d. Additionally, the resistance signal of the multifunctional ionization layer shows excellent stability within a consistent humidity range, as depicted in Figure 3e. Reproducibility is assessed by real-time recording of $\Delta R/R_0$ during periodic moisture loading and unloading

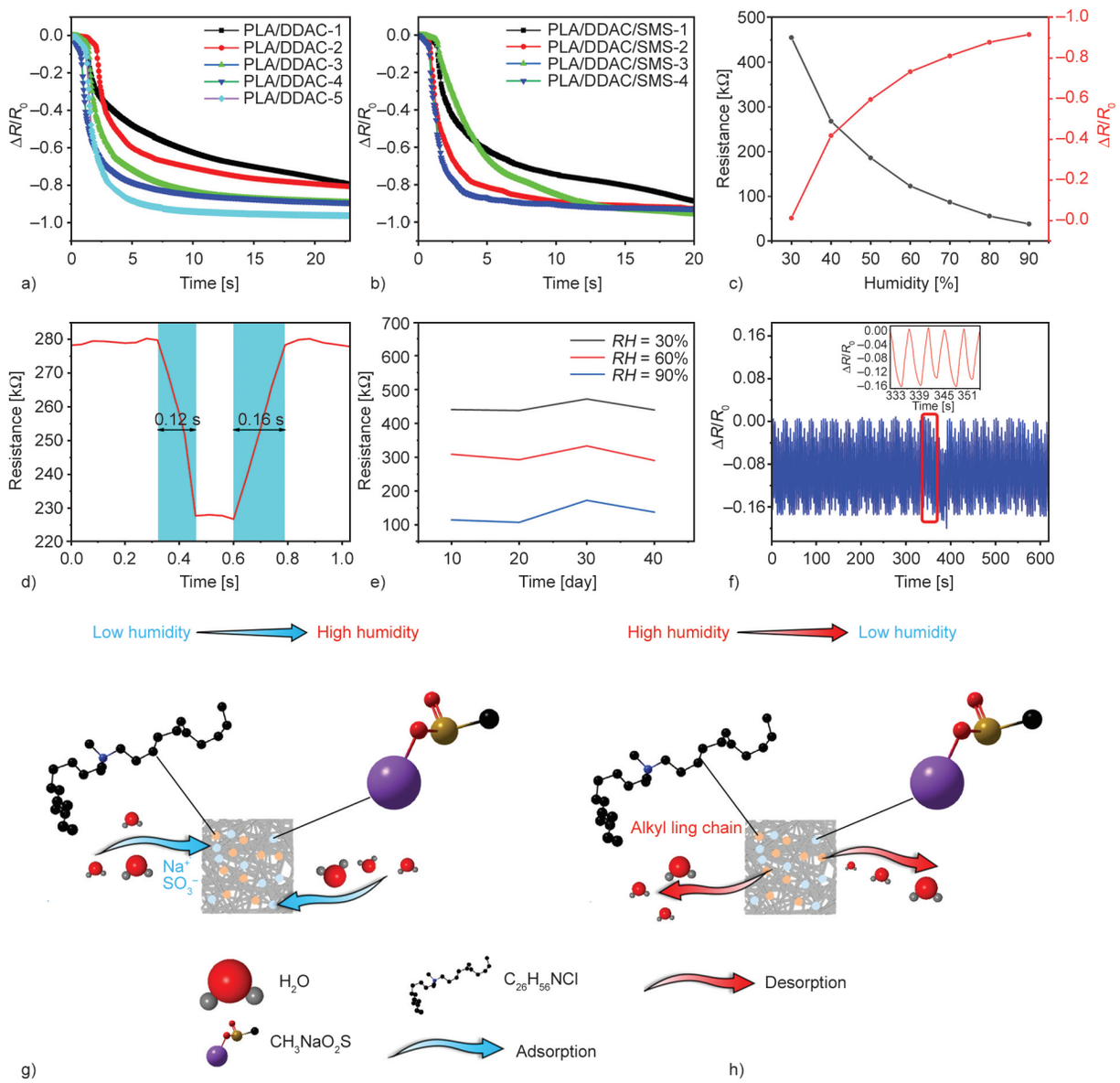

Figure 3. Sensing mechanism of the PLA/DDAC/SMS surgical mask sensor. a) Effect of DDAC concentration on moisture detection. b) Impact of DDAC/SMS concentration on $\Delta R/R_0$ variation. c) $\Delta R/R_0$ and resistance behaviors of the PLA/DDAC/SMS sensor with changes in humidity. d) Sensitivity of the PLA/DDAC/SMS sensor during the respiratory process. e) Resistance stability of the PLA/DDAC/SMS sensor at different humidity levels: 30, 60, and 90%. f) Reproducibility test of the PLA/DDAC/SMS sensor at 60% humidity over 40 cycles. g) Interaction between H_2O and DDAC/SMS from low to high humidity. h) Interaction between H_2O and DDAC/SMS from high to low humidity.

cycles at 60% humidity. The output resistance signal remains nearly unchanged after 600 s (Figure 3f). Importantly, a model is proposed to explain the sensing mechanism, as illustrated in Figures 3g and 3h. The breathing process in real-world scenarios can be classified into 'low-to-high humidity' and 'high-to-low humidity' conditions. In a low-to-high humidity environment, the polar SMS rapidly adsorbs water molecules and quickly reaches a dynamic equilibrium, and corresponding conclusions have also been reported [39]. In a high-to-low humidity environment, the alkyl chain facilitates the desorption of water molecules. During this process, a liquid layer forms around the polymer film, and H_3O^+ ions are produced by the dissociation of adsorbed water.

Figure 4 illustrates the use of the ionic salt-modified PLA textile sensor in a surgical mask for detecting physiological activities such as breathing and coughing. As shown in Figure 4a, the sensor is attached to a mask and exposed to human respiration. The sensor signal, depicted in Figure 4b, can detect both coughing and rapid breathing. We monitored the relative humidity (*RH*) from nasal breath rather than from the mouth, as nasal breath provides a more accurate measure of lung hydration levels without interference from saliva. The results indicate that coughs, characterized by stronger airflow, can be statistically distinguished from regular respiration based on changes in resistance values. Additionally, the waveform for fast breathing fluctuates more frequently than that for normal breathing. According to previous reports, one complete respiratory cycle, from exhaling (T_n^{Ex}) to inhaling (T_n^{In}), and the respiratory rate in each breath cycle were calculated as follows (Equation 3) [40]:

$$R_{res} = \frac{60}{T_n^{Ex} + T_n^{In}} \left[\frac{\text{breaths}}{\text{min}}\right] \quad (3)$$

Figure 4c shows normal breathing, with the respiratory rate calculated as approximately 16 breaths/min

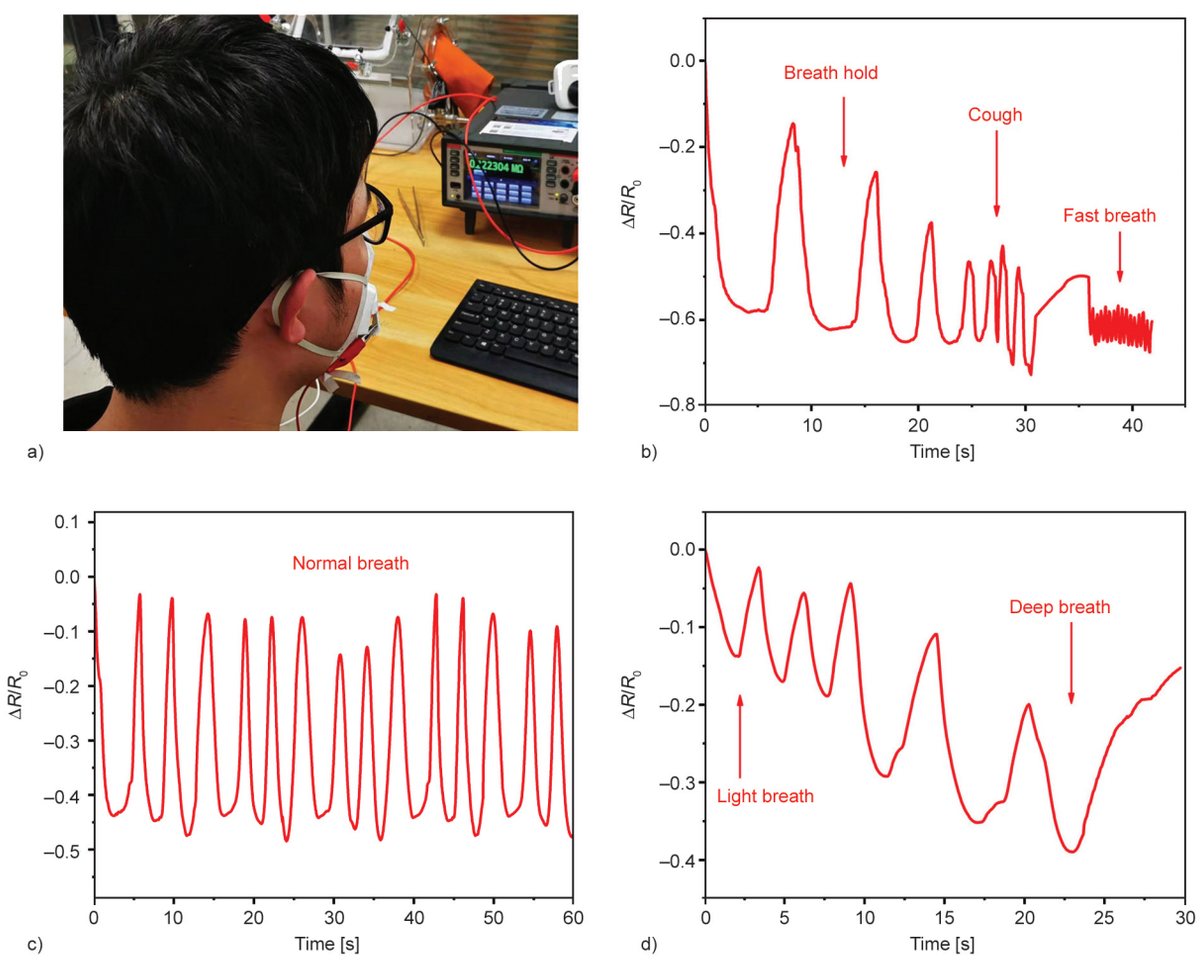

Figure 4. Respiratory application of the PLA/DDAC/SMS surgical mask sensor. a) Schematic diagram of the PLA/DDAC/SMS surgical mask sensor in a respiratory application. b) Detection of normal breath, cough, and rapid breath. c) Reproducibility of the sensor's response to normal breath. d) Detection of light breath and deep breath.

using Equation (1), consistent with the normal adult rate of 16–18 breaths/min. Additionally, both light and deep breathing can be detected, as shown in Figure 4d. Therefore, the mask is capable of simultaneously monitoring both exhaled flow humidity and respiratory rate in real time.

3.3. Self-sterilization of salt modified PLA textile

Figure 5 illustrates the antimicrobial activity of the salt-modified PLA textile composite, which displays markedly different antibacterial properties. PLA fabric control samples show no significant biocidal effects. However, after exposure to *E. coli* and *S. aureus* for a period, the PLA/DDAC/SMS samples effectively reduced bacterial counts to zero, achieving a total sterilization of 104 CFU/ml (Figure 5a). Remarkably, PLA/DDAC/SMS exhibited reductions of 99.9% against both *E. coli* and *S. aureus* after 1 h of contact. The bacterial reduction against *E. coli* increased significantly to 6 logs, while the reduction against *S. aureus* slightly rose to 4.7 logs. The relationship between antimicrobial activity and contact time is shown in Figure 5b. This indicates that a low loading of DDAC can exhibit superior antimicrobial properties. The PLA/DDAC/SMS demonstrates stronger antimicrobial performance against Gram-positive *S. aureus* compared to Gram-negative *E. coli*. Figure 5c shows both *S. aureus* and *E. coli* before and after treatment with PLA/DDAC/SMS, revealing almost no viable bacterial colonies. Additionally, the antibacterial mechanism of PLA/DDAC/SMS is detailed in Figure 5d. The quaternary ammonium cationic groups on the surface of PLA/DDAC/SMS

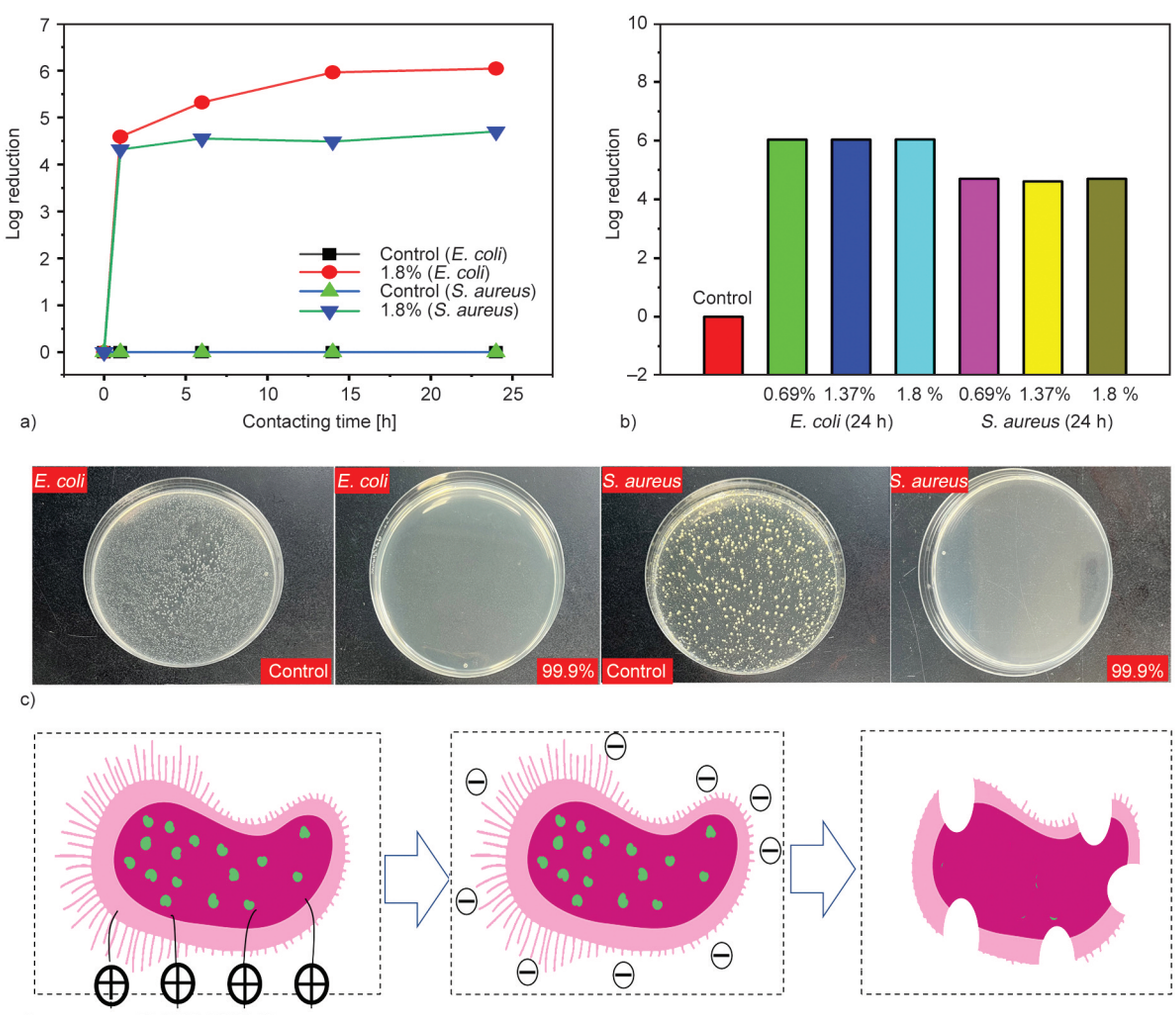

Figure 5. Self-sterilization of the PLA/DDAC/SMS surgical mask. a) Comparison of antimicrobial activity of PLA/DDAC/SMS against *E. coli* and *S. aureus*. b) Effect of DDAC concentration on antimicrobial activity against *E. coli* and *S. aureus*. c) Comparison of inhibition test results for *E. coli* and *S. aureus*. d) Antibacterial mechanism of PLA/DDAC/SMS.

bind to the negatively charged bacterial membranes [38], while the long alkyl chains of SMS disrupt the cell membranes [24], leading to leakage of cytoplasmic components and ultimately deactivating the bacteria, resulting in potent antimicrobial activity.

3.4. Degradation property of salt-modified PLA textile

Figure 6 shows the degradation properties of PLA/DDAC/SMS surgical masks during soil burial hydrolytic degradation. The pure PLA and PLA/DDAC/SMS surgical masks exhibit distinctly different degradation behaviors, as shown in Figure 6a. The excellent biodegradability of PLA/DDAC/SMS is attributed to the hygroscopicity of the ammonium cationic group and Na^+, which effectively facilitate the hydrolysis process [18]. Figure 6b illustrates the morphological changes of pure PLA and PLA/DDAC/SMS after 30 and 90 days. Figure 6c shows the acid degradation behavior of pure PLA and PLA/DDAC/SMS, with pure PLA showing a mass loss rate of around 2.57%, while PLA/DDAC/SMS reaches up to 60.38% after 30 days. Similarly, Figure 6d demonstrates the alkaline degradation behavior of both materials.

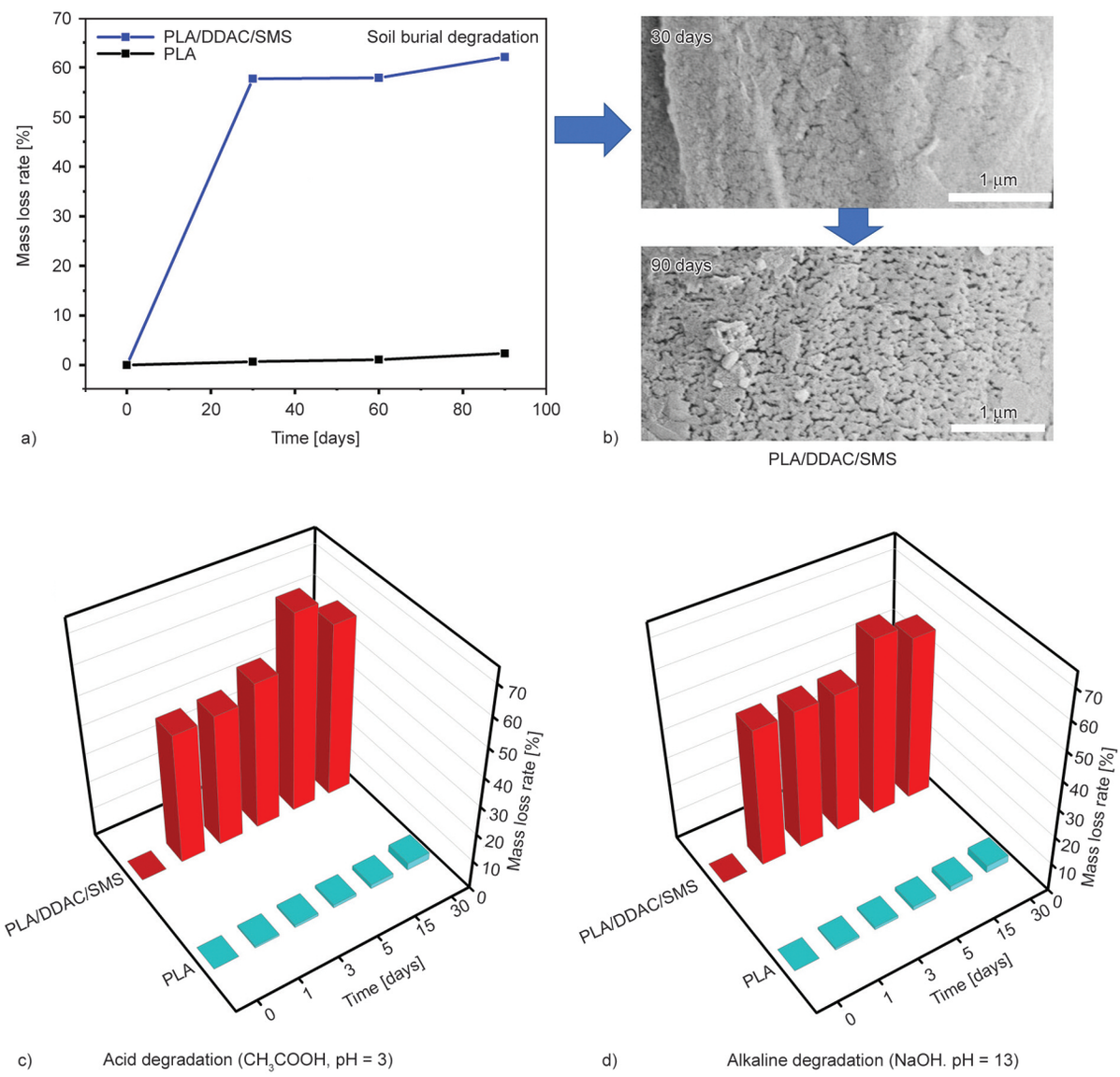

Figure 6. Degradation property of PLA/DDAC/SMS surgical mask. a) The mass loss rate comparison between PLA/DDAC/SMS and PLA on soil burial degradation. b) SEM images of the PLA/DDAC/SMS on 30 and 90 days. c) The acid degradation effected on PLA/DDAC/SMS and PLA. d) The alkaline degradation effected on PLA/DDAC/SMS and PLA.

4. Conclusions

In summary, we present a multifunctional ionic salt modification strategy for PLA textile that not only enhances respiratory detection and antibacterial properties but also promotes efficient degradation. The modified PLA textile sensor exhibits high sensitivity to respiratory humidity (0.92 at 90% *RH*), with ultrafast response (0.12 s) and recovery times (0.16 s). Additionally, the textile demonstrates excellent antibacterial performance against both *E. coli* (99.9%) and *S. aureus* (99.9%) after 1 h of contact. It also shows notable biodegradability with a weight loss rate of 60.38% after 30 days. The novel organic salt-modified PLA textile strategy offers a new approach to mitigating the severe risks of disease transmission and environmental pollution associated with non-degradable PP disposable masks.

Acknowledgements

This work was financially supported by the National Nature Science Foundation of China (52103255), Guangdong Basic and Applied Basic Research Foundation (2022A1515240005), Dongguan Sci-tech Commissioner Program (2304004020), Research Start-up Funds of DGUT (211135130).

References

[1] Umar Y., Al-Batty S., Rahman H., Ashwaq O., Sarief A., Sadique Z., Sreekumar P. A., Haque S. K. M.: Polymeric materials as potential inhibitors against SARS-CoV-2. Journal of Polymers and the Environment, **30**, 1244–1263 (2021). https://doi.org/10.1007/s10924-021-02272-6

[2] Liu L., Luo T., Kuang X., Wan X., Liang X., Jiang G., Cong H., He H.: Analysis and optimization of electrospinning parameters for fabricating thermoplastic polyurethanes (TPU) nanofibers by response surface methodology. Express Polymer Letters, **18**, 807–818 (2024). https://doi.org/10.3144/expresspolymlett.2024.60

[3] Zhang N., Wang L., Deng X., Liang R., Su M., He C., Hu L., Su Y., Ren J., Yu F., Du L., Jiang S.: Recent advances in the detection of respiratory virus infection in humans. Journal of Medical Virology, **92**, 408–417 (2020). https://doi.org/10.1002/jmv.25674

[4] Tuñón-Molina A., Takayama K., Redwan E. M., Uversky V. N., Andrés J., Serrano-Aroca Á.: Protective face masks: Current status and future trends. ACS Applied Materials and Interfaces, **13**, 56725–56751 (2021). https://doi.org/10.1021/acsami.1c12227

[5] Gong J., Fu Z., Zhou S., Zhang C., Zhu N., Wang X., Zhou Z., Liu X., Xia L., Xu W.: A facile strategy for rapid *in situ* synthesis of Cu_2O on PP non-woven fabric with durable antibacterial activities. Composites Communications, **34**, 101271 (2022). https://doi.org/10.1016/j.coco.2022.101271

[6] Gu C., Qin W., Wang Y., Li X., Wang J., Tian Z., Yang M., Qiao H., Wu Y., Yin S.: Highly stretchable, durable, and superfine fiber-shaped strain sensor with a porous core-sheath microstructure. Composites Communications, **36**, 101381 (2022). https://doi.org/10.1016/j.coco.2022.101381

[7] El Fazdoune M., Bahend K., Oubella M., Ben Jadi S., El Guerraf A., Bazzaoui E. A., García-García F. J., Martinis J. I., Bazzaoui M.: Poly(methylene blue) modified PLA-CB conductive 3D printer filament as a promising platform for electrochemical sensing of uric acid. Journal of Polymers and the Environment, **32**, 2105–2119 (2023). https://doi.org/10.1007/s10924-023-03100-9

[8] Demirtaş M. S., Saha M. C.: Engineering highly aligned continuous nanofibers *via* electrospinning: A comprehensive study on collector design, electrode geometry, and collector speed. Express Polymer Letters, **18**, 851–867 (2024). https://doi.org/10.3144/expresspolymlett.2024.63

[9] Orooji Y., Sohrabi H., Hemmat N., Oroojalian F., Baradaran B., Mokhtarzadeh A., Mohaghegh M., Karimi-Maleh H.: An overview on SARS-CoV-2 (COVID-19) and other human coronaviruses and their detection capability *via* amplification assay, chemical sensing, biosensing, immunosensing, and clinical assays. Nano-Micro Letters, **13**, 18 (2020). https://doi.org/10.1007/s40820-020-00533-y

[10] Soto F., Ozen M. O., Guimarães C. F., Wang J., Hokanson K., Ahmed R., Reis R. L., Paulmurugan R., Demirci U.: Wearable collector for noninvasive sampling of SARS-CoV-2 from exhaled breath for rapid detection. ACS Applied Materials and Interfaces, **13**, 41445–41453 (2021). https://doi.org/10.1021/acsami.1c09309

[11] Wang W., Zhang T., Fang H., Zhang Z., Peng Z., Wang Z., Ai J., Zhang F.: Structural and dimensional engineering of three-dimensional carbon nanotube/polydimethylsiloxane composite for stretchable sensor. Composites Communications, **44**, 101755 (2023). https://doi.org/10.1016/j.coco.2023.101755

[12] Gusmão A. P., Rosenberger A. G., Muniz E. C., Dragunski D. C., Caetano J.: Characterization of microfibers of carbon nanotubes obtained by electrospinning for use in electrochemical sensor. Journal of Polymers and the Environment, **29**, 1551–1565 (2020). https://doi.org/10.1007/s10924-020-01964-9

[13] Zhao P., Song Y., Xie P., Zhang F., Xie T., Liu G., Zhao J., Han S-T., Zhou Y.: All-organic smart textile sensor for deep-learning-assisted multimodal sensing. Advanced Functional Materials, **33**, 2301816 (2023). https://doi.org/10.1002/adfm.202301816

[14] Varanges V., Caglar B., Lebaupin Y., Batt T., He W., Wang J., Rossi R. M., Richner G., Delaloye J. R., Michaud V.: On the durability of surgical masks after simulated handling and wear. Scientific Reports, **12**, 4938 (2022). https://doi.org/10.1038/s41598-022-09068-1

[15] Khan A. A. P., Khan A., Rahman M. M., Asiri A. M., Oves M.: Chemical sensor development and antibacterial activities based on polyaniline/gemini surfactants for environmental safety. Journal of Polymers and the Environment, **26**, 1673–1684 (2017). https://doi.org/10.1007/s10924-017-1055-9

[16] Xiong S-W., Fu P-G., Zou Q., Chen L-Y., Jiang M-Y., Zhang P., Wang Z-G., Cui L-S., Guo H., Gai J-G.: Heat conduction and antibacterial hexagonal boron nitride/polypropylene nanocomposite fibrous membranes for face masks with long-time wearing performance. ACS Applied Materials and Interfaces, **13**, 196–206 (2021). https://doi.org/10.1021/acsami.0c17800

[17] Lee S., Nam J-S., Han J., Zhang Q., Kauppinen E. I., Jeon I.: Carbon nanotube mask filters and their hydrophobic barrier and hyperthermic antiviral effects on SARS-CoV-2. ACS Applied Nano Materials, **4**, 8135–8144 (2021). https://doi.org/10.1021/acsanm.1c01386

[18] Musioł M., Rydz J., Sikorska W., Janeczek H., Jurczyk S.: Organic recycling challenges of (bio)degradable packages: Degradation studies of polylactide/cork composites. Express Polymer Letters, **18**, 868–880 (2024). https://doi.org/10.3144/expresspolymlett.2024.64

[19] Zhong H., Zhu Z., Lin J., Cheung C. F., Lu V. L., Yan F., Chan C-Y., Li G.: Reusable and recyclable graphene masks with outstanding superhydrophobic and photothermal performances. ACS Nano, **14**, 6213–6221 (2020). https://doi.org/10.1021/acsnano.0c02250

[20] Serrano-Aroca Á.: Antiviral characterization of advanced materials: Use of bacteriophage phi 6 as surrogate of enveloped viruses such as SARS-CoV-2. International Journal of Molecular Sciences, **23**, 5335 (2022). https://doi.org/10.3390/ijms23105335

[21] Lustig S. R., Biswakarma J. J. H., Rana D., Tilford S. H., Hu W., Su M., Rosenblatt M. S.: Effectiveness of common fabrics to block aqueous aerosols of virus-like nanoparticles. ACS Nano, **14**, 7651–7658 (2020). https://doi.org/10.1021/acsnano.0c03972

[22] Ren Q., Yu N., Zou P., He Q., Macharia D. K., Sheng Y., Zhu B., Lin Y., Wu G., Chen Z.: Reusable $Cu_{2-x}S$-modified masks with infrared lamp-driven antibacterial and antiviral activity for real-time personal protection. Chemical Engineering Journal, **441**, 136043 (2022). https://doi.org/10.1016/j.cej.2022.136043

[23] Marković D., Tseng H-H., Nunney T., Radoičić M., Ilic-Tomic T., Radetić M.: Novel antimicrobial nanocomposite based on polypropylene non-woven fabric, biopolymer alginate and copper oxides nanoparticles. Applied Surface Science, **527**, 146829 (2020). https://doi.org/10.1016/j.apsusc.2020.146829

[24] Kumaran S., Oh E., Han S., Choi H-J.: Photopolymerizable, universal antimicrobial coating to produce high-performing, multifunctional face masks. Nano Letters, **21**, 5422–5429 (2021). https://doi.org/10.1021/acs.nanolett.1c00525

[25] Krainoi A., Boonkerd K.: Mechanical/electrical properties and strain sensibility of epoxidized natural rubber nanocomposite filled with carbon nanotube: Effect of sodium alginate as a surfactant on latex technology process. Express Polymer Letters, **17**, 850–866 (2023). https://doi.org/10.3144/expresspolymlett.2023.63

[26] Soni R., Joshi S. R., Karmacharya M., Min H., Kim S-K., Kumar S., Kim G-H., Cho Y-K., Lee C. Y.: Superhydrophobic and self-sterilizing surgical masks spray-coated with carbon nanotubes. ACS Applied Nano Materials, **4**, 8491–8499 (2021). https://doi.org/10.1021/acsanm.1c01082

[27] Zheng X., Zhang S., Zhou M., Lu H., Guo S., Zhang Y., Li C., Tan S. C.: MXene functionalized, highly breathable and sensitive pressure sensors with multi-Layered porous structure. Advanced Functional Materials, **33**, 2214880 (2023). https://doi.org/10.1002/adfm.202214880

[28] Konda A., Prakash A., Moss G. A., Schmoldt M., Grant G. D., Guha S.: Aerosol filtration efficiency of common fabrics used in respiratory cloth masks. ACS Nano, **14**, 6339–6347 (2020). https://doi.org/10.1021/acsnano.0c03252

[29] Ounkaew A., Kasemsiri P., Srichiangsa N., Jetsrisuparb K., Knijnenburg J. T. N., Okhawilai M., Hiziroglu S., Theerakulpisut S.: Multifunctional gluten/guar gum copolymer with self-adhesion, self-healing, and remolding properties as smart strain sensor and self-powered device. Express Polymer Letters, **16**, 607–623 (2022). https://doi.org/10.3144/expresspolymlett.2022.45

[30] Song Y. X., Xu W. M., Rong M. Z., Zhang M. Q.: A sunlight self-healable fibrous flexible pressure sensor based on electrically conductive composite wool yarns. Express Polymer Letters, **14**, 1089–1104 (2020). https://doi.org/10.3144/expresspolymlett.2020.88

[31] Zhang S., Andre J. S., Hsu L., Toolis A., Esarey S. L., Li B., Chen Z.: Nondestructive *in situ* detection of chemical reactions at the buried interface between polyurethane and isocyanate-based primer. Macromolecules, **53**, 10189–10197 (2020). https://doi.org/10.1021/acs.macromol.0c01862

[32] Allison L. K., Rostaminia S., Kiaghadi A., Ganesan D., Andrew T. L.: Enabling longitudinal respiration monitoring using vapor-coated conducting textiles. ACS Omega, **6**, 31869–31875 (2021). https://doi.org/10.1021/acsomega.1c04616

[33] Bhati V. S., Kumar M., Banerjee R.: Gas sensing performance of 2D nanomaterials/metal oxide nanocomposites: A review. Journal of Materials Chemistry C, **9**, 8776–8808 (2021). https://doi.org/10.1039/d1tc01857d

[34] Choo J. E., Kim D. Y., Park T. H., Hwang S. W.: Influence of modified poly(glycolic acid) on the physical and mechanical properties of PLA/PBAT/mPGA multiphase blends. Journal of Polymers and the Environment, **32**, 3089–3103 (2024). https://doi.org/10.1007/s10924-023-03150-z

[35] Dai J., Zhao H., Lin X., Liu S., Liu Y., Liu X., Fei T., Zhang T.: Ultrafast response polyelectrolyte humidity sensor for respiration monitoring. ACS Applied Materials and Interfaces, **11**, 6483–6490 (2019). https://doi.org/10.1021/acsami.8b18904

[36] Muzata T. S., Gebrekrstos A., Ray S. S.: Recent progress in modified polymer-based PPE in fight against COVID-19 and beyond. ACS Omega, **6**, 28463–28470 (2021). https://doi.org/10.1021/acsomega.1c04754

[37] Peter A., Cozmuta L. M., Nicula C., Cozmuta A. M., Drazic G., Peñas A., Silvi S.: Recovery and characterization of nano-ag-graphene-TiO_2: Active compound from polylactic acid (PLA)-based film. Journal of Polymers and the Environment, **32**, 133–149 (2023). https://doi.org/10.1007/s10924-023-02995-8

[38] Jennings M. C., Minbiole K. P. C., Wuest W. M.: Quaternary ammonium compounds: An antimicrobial mainstay and platform for innovation to address bacterial resistance. ACS Infectious Diseases, **1**, 288–303 (2015). https://doi.org/10.1021/acsinfecdis.5b00047

[39] Estillore A. D., Hettiyadura A. P. S., Qin Z., Leckrone E., Wombacher B., Humphry T., Stone E. A., Grassian V. H.: Water uptake and hygroscopic growth of organosulfate aerosol. Environmental Science and Technology, **50**, 4259–4268 (2016). https://doi.org/10.1021/acs.est.5b05014

[40] He J., Xiao P., Shi J., Liang Y., Lu W., Chen Y., Wang W., Théato P., Kuo S-W., Chen T.: High performance humidity fluctuation sensor for wearable devices *via* a bioinspired atomic-precise tunable graphene-polymer heterogeneous sensing Junction. Chemistry of Materials, **30**, 4343–4354 (2018). https://doi.org/10.1021/acs.chemmater.8b01587